Aerodynamic Optimization Trade Study of a Box-Wing Aircraft Configuration

Hugo Gagnon[1] and David W. Zingg[2]
University of Toronto, Toronto, Ontario M3H 5T6, Canada

This study investigates the aerodynamic trade-offs of a box-wing aircraft configuration using high-fidelity aerodynamic optimization. A total of five optimization studies are conducted, where each study extends the previous one by progressively adding a combination of design variables and constraints. Examples of design variables include wing twist and sectional shape; examples of constraints include trim and stability requirements. In all cases the objective is to minimize inviscid drag at a prescribed lift and a Mach number of 0.78. Aerodynamic functionals are evaluated based on the discrete solution of the Euler equations, which are tightly coupled with an adjoint methodology incorporating a gradient-based optimizer. For each study an equivalent conventional tube-and-wing baseline is similarly optimized in order to enable direct comparisons. It is found that the transonic box-wing aircraft considered here, whose height-to-span ratio is about 0.2, produces up to 43% less induced drag than its conventional counterpart. The unique capability of the box wing to redistribute its optimal lift distribution contributes significantly to this benefit as it enables trim and other constraints to be satisfied with almost no performance degradation. The impact of nonlinear aerodynamics on the box wing is explored further through a series of subsonic optimization studies.

Nomenclature

b	wing span

[1] Currently Development Engineer, NUMECA International. Member AIAA.
[2] Professor and Director, Institute for Aerospace Studies, Tier 1 Canada Research Chair in Computational Aerodynamics and Environmentally Friendly Aircraft Design, J. Armand Bombardier Foundation Chair in Aerospace Flight. Associate Fellow AIAA.

c	root chord
C_L	lift coefficient
e	span efficiency
h	wing vertical extent
L, D	lift and drag (half geometry)
M_x, M_y	bending and pitching moments (half geometry)
M_∞	freestream Mach number
q_∞	freestream dynamic pressure
R	corner fillet radius
S	reference area
W	weight
x, y, z	chordwise, spanwise, and vertical coordinates
α	angle of attack
η, η_V	normalized wing semi-span and vertical coordinates

Acronyms

BW	Box Wing
cg	center of gravity
np	neutral point
TW	Tube-and-Wing

I. Introduction

In a 1924 NACA report, Ludwig Prandtl reasoned that a biplane joined by end plates corresponds to a solution of minimum induced drag for a fixed lift, span, and vertical extent [1]. He called this solution the "Best Wing System". In the same report Prandtl also gives an approximate procedure with which to estimate the span efficiency of such box-wing systems. For example, for a height-to-span (h/b) ratio of 0.3, an optimally-loaded box wing should only generate 60% of the induced drag of a monoplane of the same span and lift. A 24% overall drag reduction (60% of 40%, the proportion of induced drag on a typical aircraft

at cruise [2]) of the current worldwide aircraft fleet would not only save the industry billions of U.S. dollars every year, but also significantly reduce fuel consumption and hence help mitigate climate change [3]. Yet, to this day, 91 years after Prandtl's discovery, no commercial box-wing aircraft has ever been built.

One of the first attempts to adapt the box-wing design to a transonic transport was initiated at Lockheed in the early 1970s, first by Miranda [4], then by Lange *et al.* [5]. While Miranda successfully retrieved the expected induced drag savings predicted by linear theory, the ensuing feasibility study of Lange *et al.* on a Mach 0.95 "boxplane" uncovered a series of unforeseen problems. Chief among these was the appearance of both symmetric and antisymmetric instabilities well below the target flutter speed. At that time the adopted design solution comprised a gull-like inboard section on the rear-mounted swept-forward upper wing (thus permitting the installation of a V-tail), and a root-chord extension on the forward-mounted swept-back lower wing (thus permitting a lighter structure). Still, Lange *et al.* concluded that no ramp weight reduction over a conventional baseline could be achieved, and that the boxplane might only be advantageous at lower Mach numbers (for which case the flutter speed requirement would not be as stringent).

More recently, the "PrandtlPlane" of Frediani [6] has revived the box-wing configuration as a viable alternative to the ubiquitous tube-and-wing, not just for potential commercial applications, but also for personal use [7]. Analogous to Lange *et al.* [5], his solution to dominate early flutter onset is to use twin-fins that are maximally distanced apart [8], implying wider than usual aft fuselage cross-sections. According to a related study, see [9], it is also possible to build a metallic box wing that is aeroelastically stable and that has roughly the same wing weight to maximum take-off weight ratio (W_{wing}/MTOW) as a conventional wing, provided the wing box is carefully designed. Examples of design guidelines include reinforcing the cross-section flanges in the out-of-plane axis while weakening the other direction. Similar guidelines were also given by Wolkovitch [10], who, working on the joined wing,[1] added that the effective beam depth of such systems is primarily determined by airfoil chord rather than thickness. Other studies that focus on the structural implications of box wings include [11] and [12].

Assuming the structural challenges associated with the design of box wings are surmountable, questions related to practical aerodynamics are still open-ended. First, for a fixed span, even though the wetted area of

[1] In this paper a distinction between joined and box wings is made; whereas a box wing has vertical fins attaching its lower and upper wings at their tip, a joined wing has no such tip fins and thus appears diamond-shaped from both the front and top views.

a box wing is exactly the same as a conventional wing-plus-tail configuration, the local Reynolds numbers will, on average, be halved, resulting in a total friction drag on the box wing higher than on the conventional wing-plus-tail. Second, joined and box wings alike have been observed to exhibit nose-down characteristics at moderate angles of attack (owing to the front wing stalling first, thus reducing the downwash on the rear wing, which in turn causes an increase of the pitch-down moment contribution of the rear wing) [10]. While desirable for safety reasons, this reflex mechanism can severely limit the maximum attainable lift. As noted by Addoms and Spaid [13], "biplane configurations must employ airfoils having substantially different camber from those of competitive monoplanes". Although the present study does not account for flow separation, it does account for the flow curvature induced by the neighboring wings.

The objectives of this work are 1) to gain a better understanding of the aerodynamic trade-offs involved in the design of box wings by conducting a series of high-fidelity aerodynamic shape optimization trade studies of increasing complexity, and 2) to compare, on the basis of absolute inviscid pressure drag at transonic speeds, the optimized box wing (BW) against a similarly optimized conventional tube-and-wing (TW). While our models do not account for structures, we do ensure that all designs have, for example, sufficient internal volume and thickness-to-chord ratios. Our hope is that, by including nonlinear effects as captured by the Euler equations, subtle yet important trends will arise as a result of the optimizations that are otherwise undetectable by commonly used low-fidelity models [14].

The remainder of this paper proceeds by first introducing the chosen BW and reference TW aircraft configurations in Sec. II A, after which the optimization problems are formulated in Sec. II B. Section II C briefly reviews the methodology, including the shape parameterization and control techniques employed for the aerodynamic shape optimization studies of Sec. III. Section III also contains a preliminary study investigating the effect of the target lift and h/b ratio on the span efficiency and force distribution of a NACA-0012 BW geometry at subsonic speed. Finally, conclusions and future work are discussed in Sec. IV.

II. Problem Setup and Methodology

A. Initial Geometry

The BW aircraft studied in this work is intended to perform a regional mission consisting of carrying 100 passengers and 3 crew members over 926 km ($\sim$ 500 nm) at Mach 0.78 and an altitude of 10.5 km ($\sim$

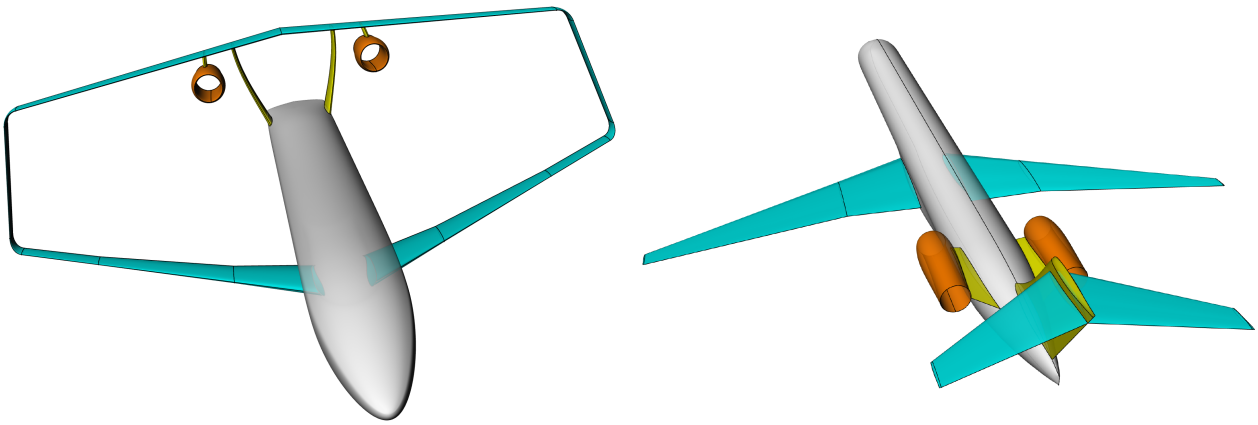

(a) box wing (BW) (b) tube-and-wing (TW)

Fig. 1 Outer mold line of the BW and reference TW regional jets.

35,000 ft). The reference TW aircraft is the Bombardier CRJ1000 NextGen.[2] The initial outer mold line geometries of both configurations are shown in Fig. 1. Compared to the TW, the BW has wider fuselage cross-sections which allows for the installation of the structurally efficient twin-fins mentioned in Sec. I. The wider fuselage also allows for a 3-2 seating arrangement (as opposed to 2-2 for the TW); hence, for the same capacity the BW is also shorter: 34.31 m compared to 38.77 m for the TW. For a given wing span and sweep, the shorter fuselage allows the longitudinal spread of the top and bottom wings to be increased without resorting to overly swept-back tip fins. Maximizing the distance between the two wings helps keep the center of gravity in the middle which improves elevator effectiveness [6].

Only the main lifting surfaces of each configuration (partially shown in cyan in Fig. 1) are included in the aerodynamic analysis of the optimization studies. Figure 2 shows the lifting surfaces of the BW aircraft configuration. The planform is adapted from the one in [6]. The h/b ratio is 0.2278 at the root and 0.1858 at the tip, averaging to about 0.2. The span of 26.2 m is chosen to match the span of the reference TW aircraft [15]. As specified in Table 1 the wetted area of the BW is also relatively similar to that of the TW. This is important if the BW is to be competitive from the perspective of viscous drag. Note that the wetted areas reported here are those of the wing systems alone, i.e. of the wing-loop for the BW (Fig. 2) and of the wing-plus-tail for the TW. In contrast, the wetted area of the full (watertight) aircraft is used in the calculation of the empty manufacturing weights [16]. The propulsion, systems, operational, payload, and fuel load groups

[2] Data available online at http://commercialaircraft.bombardier.com/en/crj.html [retrieved 1 May 2015]

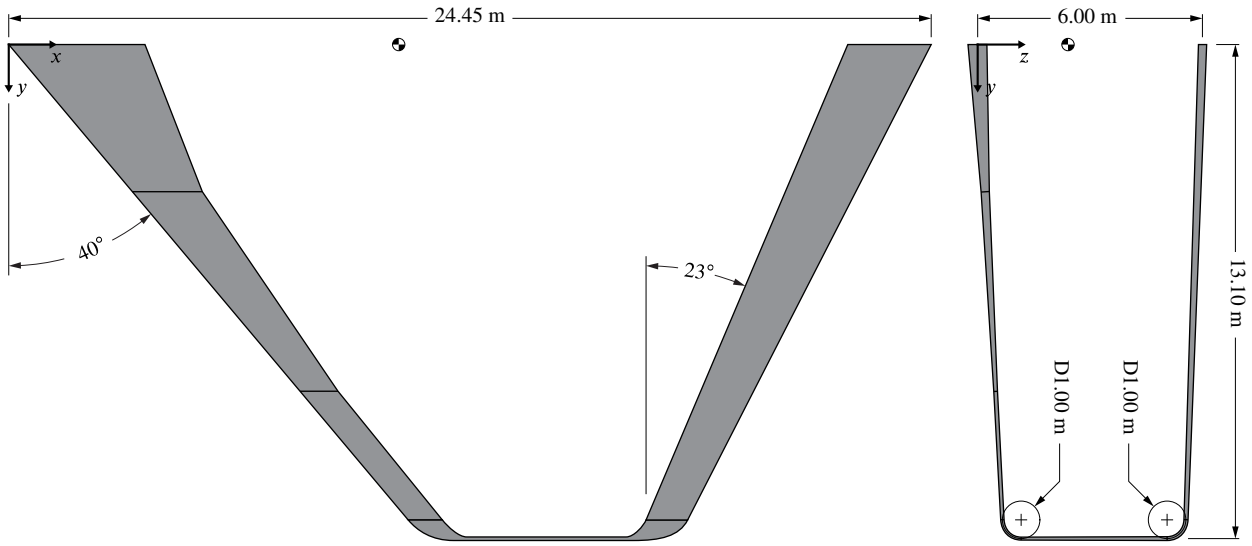

(a) top (b) front

Fig. 2 Top and front views of the BW aircraft configuration.

Table 1 Geometry and grid data for the TW and BW aircraft

	TW	BW
geometry		
b [m]	26.2	26.2
S_{wet} [m^2]	385.73	387.82
W [N]	369,720	379,617
$(x_{\text{cg}}, z_{\text{cg}})$ [m]	$(3.67, 0)$	$(10.33, 2.41)$
grid		
blocks	126	96
nodes	4.0 M	3.4 M
blocks (fine)	2133	2141
nodes (fine)	87.8 M	88.6 M

are assumed fixed and to be the same for both aircraft. Since a larger portion of the wing is buried inside the fuselage in the case of the TW, and since the BW has two (albeit smaller) vertical stabilizers, the weight model results in a BW aircraft that is overall 2.7% heavier. We emphasize that this model is low-fidelity, but

we nevertheless believe it to be accurate enough so to not significantly influence the conclusions of this work. For the BW the wetted area of the full aircraft is also used to compute the initial location of its center of gravity; for the TW, the center of gravity is fixed at 25% of the mean aerodynamic chord, which corresponds to 3.67 m as measured from the leading edge root.

The wing geometries are generated by linearly interpolating two tip airfoils between each wing segment, resulting in watertight networks of high-quality non-uniform rational B-spline surfaces [17]. For this study only supercritical airfoils are selected [18]. Specifically, for the BW the selected airfoils are the NASA's SC(2)-0614 (bottom wing root), -0412 (bottom wing mid section root), -0410 (bottom wing mid section tip and top wing root to tip), and -0010 (vertical tip fin); for the TW, the selected airfoils are the NASA's SC(2)-0614 (root), -0412 (crank), and -0410 (tip and tail root to tip). In both cases the angle of attack relative to the x axis (i.e. to the fuselages) is fixed at 0 and the wings are initially untwisted.

B. Optimization Problem Formulation

In order to draw direct comparisons on the basis of total (inviscid) drag, it is essential that both the BW and reference TW aircraft configurations be optimized in similar fashion, i.e. with the same objective function and with consistent sets of design variables and constraints.

1. *Objective Function*

All of the aerodynamic design optimization studies presented in this work, including the preliminary study on the NACA-0012 geometry (Sec. III A), are drag minimization problems. Since only single-point optimizations are conducted, the most critical point of the cruise segment is picked, i.e. at the beginning where the required lift is maximum. As discussed in Sec. II B 3, lift is constrained in each case to meet a specified target and the wing span cannot change throughout any of the optimizations; thus, an equivalent objective is to maximize span efficiency,

$$e = \frac{(L/q_\infty)^2}{\pi b^2 (D/q_\infty)}, \tag{1}$$

where here L and D correspond to the full-geometry lift and drag values, respectively, and q_∞ is the freestream dynamic pressure.

2. *Design Variables*

Inviscid pressure drag is composed of induced and wave drag components. In this work these two drag components are tackled simultaneously by enabling twist and sectional shape design variables (an overview of the geometry control methodology is given in Sec. II C 1). For the BW configuration, a total of 26 twist design variables are evenly distributed along the half-wing geometry, including the corner fillets and vertical tip fin. Also evenly distributed are the sectional shape design variables; in all, there are 520 of them, for a total of 546 geometric design variables. Similarly, there are 14 design variables parameterizing the twist (wing-plus-tail) and 200 design variables parameterizing the sectional shape (wing-only) of the TW configuration, for a total of 214 geometric design variables. Twist is applied about the leading edge of the wing segments, and the twist design variables include the angle of incidence (relative to the x axis) of the wings at the symmetry plane.

For Study 5 only (Sec. III F) the leading-edge sweep angles of the top and bottom wings are design variables. The same design variables control the sweep of the tip fin while maintaining smooth corner fillets.

Finally, given the conceptual nature of the design problem and in particular the low-fidelity of the weight and balance model, the longitudinal location of the center of gravity, x_{cg}, can also be chosen as a design variable. When doing so it is however important to enforce a proper longitudinal stability constraint, as discussed next.

3. *Constraints*

A high-fidelity aerodynamic optimization problem must be carefully constrained in order to retrieve realistic shapes. For example, if unconstrained, a single-point Euler-based optimization would result in wings with minimal internal volume and razor-thin leading edges. To address the first difficulty, an internal volume inequality constraint with a lower bound of 95% of the initial value is enforced for all cases. To address the second difficulty, the wing sections are constrained to maintain at least 60% of their original thickness at any chordwise location. For example, a wing section that is initially 10% thick cannot become less than 6% thick. Finally, twist is linearly interpolated between the two tip sections of any given wing segment, a measure that reduces the development of overly wavy surfaces in the spanwise direction and that fortunately has a minimal impact on drag.

As already mentioned in Sec. II B 1, lift is constrained to a target value for all drag minimization studies.

The target value is set to be equal to the aircraft weight at the beginning of the cruise segment. For the half-geometry BW aircraft this value corresponds to $L/q_\infty = 19.6\,\mathrm{m}^2$. When comparing the performance of different aircraft configurations it is also important that each configuration be trimmed at its design point. This is achieved here by constraining the optimizer to achieve a pitching moment, M_y, of 0 about the center of gravity. However, if the location of the center of gravity is poorly chosen, then a configuration may be overly penalized from this trim constraint. Activating x_{cg} as a design variable can help, but if such is the case then additional preventive measures must also be taken, otherwise the optimizer will simply move x_{cg} such that the constraint is satisfied. In general, moving the center of gravity aft reduces longitudinal stability, hence there is a trade-off between x_{cg}, trim, and stability. In this work we constrain longitudinal stability by forcing the center of gravity to remain at least 5% of the root-chord length ahead of the neutral point, x_{np}, i.e.

$$x_{\mathrm{np}} - x_{\mathrm{cg}} = -\frac{(M_y/q_\infty)_\alpha}{(L/q_\infty)_\alpha} \geq 0.05c, \tag{2}$$

where the α subscript denotes the partial derivative with respect to the angle of attack. Following Mader and Martins [19], these partials are evaluated using a first-order finite-difference approximation. Round-off errors can be minimized by choosing a relatively large step size (0.001°) while keeping the truncation errors within acceptable bounds, since both the pitching moment and lift are relatively linear in α for the flow regimes considered here.

The coupling between the aerodynamic and structural forces is strong in wing design, especially in the case of the BW due to its structurally overconstrained nature and potential for snap buckling [12]. While a full aerostructural shape optimization [20] is beyond the scope of this work, here we consider the center-plane bending moment as a surrogate for a structural model [21]. Specifically, the x-directional moment, M_x, about the center of gravity is constrained to be no more than 80% of the bending moment generated by the same configuration optimized without a bending moment constraint. For example, in the case of the TW, the lower bound is 80% of the bending moment generated by an elliptical lift distribution. Note that unlike the TW case, the vertical location of the center of gravity, z_{cg}, of the BW cannot be neglected since the tip fin can generate significant side-forces. An alternative would be to apply the bending moment constraint to the top and bottom wings separately, although at the time of writing it is unclear if this approach would be preferable.

C. Optimization Algorithm

The objective function, design variables, and constraints described in Sec. II B are computed by state-of-the-art optimization software collectively known as Jetstream. Many of the core components of the methodology are thoroughly described and verified in [22]; thus, only a brief summary is given here.

1. *Geometry Parameterization and Mesh Movement*

The twist, sectional shape, and planform design variables are handled by a geometry control system built around free-form and axial deformation [23]. Whereas the free-form deformation volumes (modeled as B-spline volumes) are effective at local control such as twist and sectional shape changes, the axial curves (also modeled with B-spline technology) are effective at global control such as planform changes. In general each wing segment, including the corner fillets and vertical tip fin of the BW, is assigned a single free-form deformation volume that stretches between the wing segment's tip sections. The same free-form deformation volumes are positioned such that they overlap at the tip sections. Since all free-form deformation volumes are linear in the vertical direction[3] and cubic in the other two directions, the overall wing shape is thus parameterized by piecewise-cubic polynomials in the chordwise and spanwise directions.

Following an update in the geometric design variables, the computational grid that surrounds the geometry must also deform. This is accomplished by an efficient two-level approach that models the grid as a linear elastic solid [22, 23].

2. *Flow Solver*

With the computational grid conforming to the deformed geometry, the aerodynamic functionals are evaluated based on the solution of the steady Euler equations, discretized here with second-order accurate finite-difference operators. The solution in the vicinity of shocks is stabilized by a pressure sensor mechanism involving both fourth- and second-difference scalar dissipation. The vector of nonlinear residuals is converged to a relative tolerance of 10^{-12} by an efficient parallel Newton-Krylov solver. Further details regarding the flow solver are available in [24].

---

[3] Vertical relative to the wing segment; for example, for the vertical tip fin of the BW, the vertical direction of the free-form deformation volume is along the global y axis.

Basic information on the size of the computational grids used for the optimization studies is given in Table 1. While the coarse grids are fine enough for the optimizer to capture the physics and thus correctly shape the geometry, they are nevertheless too coarse to accurately predict drag. Therefore, we perform flow analyses on fine grids before and after each optimization.

3. *Optimizer*

Jetstream relies on the gradient-based package SNOPT [25] to drive the optimization process. SNOPT uses sequential quadratic programming and is capable of handling thousands of design variables and constraints. To achieve deep convergence it is however necessary that the gradients of the functionals with respect to the design variables be accurately defined. For nonlinear constraints that do not depend on the flow, such as the internal volume, the gradients are mostly hand-differentiated. Otherwise, they are computed through the discrete-adjoint method [22, 23].

III. Aerodynamic Design Optimization Studies

We now present five drag minimization studies that investigate the effect of particular combinations of design variables and constraints on the aerodynamic performance of the transonic BW configuration. A summary of each study is given in Table 2. In each case an equivalent set of design variables and constraints is used to optimize the reference TW configuration. This is with the exception of Study 5, for which the sweep design variables are only activated on the BW configuration. For all other cases the planform of both configurations is fixed due to the absence of off-design, structural, and viscous models.

Sections III B to III F are each assigned one optimization study. In order to gain insight and confidence we first present a preliminary study on a simple NACA-0012 BW geometry. A similar study is proposed as benchmark to the 2015 AIAA Aerodynamic Design Optimization Discussion Group [26].[4]

A. NACA-0012 Box-Wing Geometry at Subsonic Speed

Under the assumption of incompressible flow, linear aerodynamic theory provides two useful results with which to compare BW optimizations. The first is an equation provided in Prandtl [1] that relates the

[4] Data available online at https://info.aiaa.org/tac/ASG/APATC/AeroDesignOpt-DG/default.aspx [retrieved 1 May 2015]

Table 2 Summary of the design variables and nonlinear constraints employed in each drag minimization study

	design variables				nonlinear constraints				
study	twist	section	sweep	x_{cg}	volume	L	M_y	M_x	$x_{np} - x_{cg}$
1	✓	✓			✓	✓			
2	✓	✓			✓	✓	✓		
3	✓	✓		✓	✓	✓	✓		✓
4	✓	✓			✓	✓		✓	
5	✓	✓	✓	✓	✓	✓	✓	✓	✓

height-to-span ratio to span efficiency:[5]

$$\frac{1}{e} \approx \frac{1 + 0.45(h/b)}{1.04 + 2.81(h/b)}. \tag{3}$$

The second is the optimal lift distribution of the BW, which is depicted by several authors (see, for instance, [5, 27]) as the sum of a constant and elliptical lift distributions equally carried by the top and bottom wings and joined at the tips by butterfly-shaped side-force distributions. A relevant problem is thus to investigate the effect of nonlinear aerodynamics on the optimal span efficiency and force distribution of the BW under a range of lift coefficients and h/b ratios. In this work we consider five lift coefficients — 0.3, 0.4, 0.5, 0.6, and 0.7 — and five h/b ratios — 0.10, 0.15, 0.20, 0.25, and 0.30. Specifically, two sets of optimizations are performed: one where the lift coefficient is varied and the height-to-span ratio is fixed at $h/b = 0.20$, and one where the lift coefficient is fixed at $C_L = 0.5$ and the h/b ratio is varied. Thus, there are a total of nine separate cases.

The generic BW geometry used for all cases is shown in Fig. 3a. The two wings and the tip fin are generated from a sharp NACA-0012 airfoil, which is rotated 90° at the wing extremities to close the system. The purpose of the corner fillets is to reduce compressibility effects. For a given h/b ratio compressibility effects can be reduced further by increasing the size of h and b relative to c. Here, R (see Fig. 3a) and b are fixed to $0.15c$ and $12c$, respectively, and h is varied from $1.2c$ to $3.6c$ by increments of $0.6c$ to generate all

[5] An approximate two-step numerical procedure that also relates h/b to e is given in Frediani and Montanari [27].

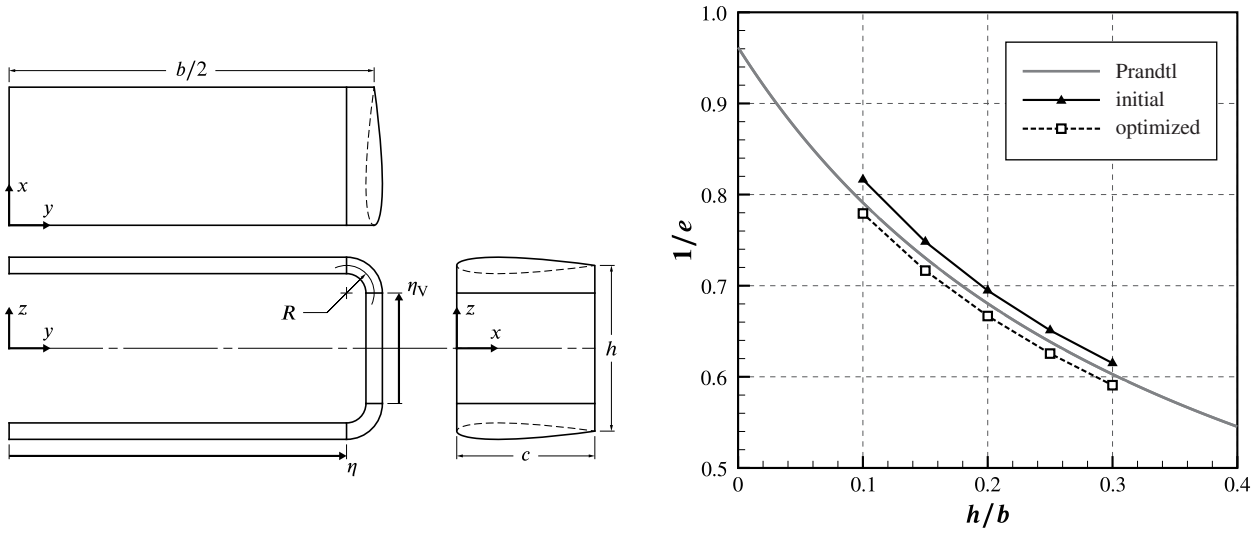

(a) generic BW geometry

(b) inverse of span efficiency versus height-to-span ratio

Fig. 3 Geometry parameterization and optimization results of the NACA-0012 BW geometry ($C_L = 0.5$).

five geometries. Note that the reference area, $S = 2bc$, is the same for each geometry and equals $24c^2$. Also note that the arc lengths of the corner fillets are excluded from the definition of the normalized semi-span (η) and vertical (η_V) coordinates.

The optimization grids are composed of 42 blocks and roughly 2.6 M nodes with off-wall spacings of about $10^{-3}c$. All five grids have the same hyperbolic mesh law parameters along the same respective block edges. As explained in Sec. II C 2, grid-converged lift and drag values are obtained by performing post-optimization flow analyses on fine grids, here composed of 2154 blocks and roughly 89.6 M nodes.

The optimization problem consists of minimizing induced drag at Mach 0.3 with respect to the twist distribution of the entire system, including the corner fillets as described below. Twist is achieved by true rotation (as opposed to shear); hence, the planform and thus the lift coefficient are not fixed. However, the target lift and angle of attack are set such that the lift coefficient is satisfied almost exactly at the beginning of the optimizations. For example, for the case where $C_L = 0.5$ and $h/b = 0.20$, the target lift is $(L/q_\infty)_{\text{target}} = (C_L \times S)/2 = (0.5 \times 24c^2)/2 = 6c^2$ and the angle of attack is $\alpha = 5.4058°$. The division by 2 is due to the half geometry.

A total of 22 free-form deformation design variables are used to achieve a continuous, piecewise-cubic twist distribution. As described in Sec. II B 2 and II C 1, twist is applied about the leading edge with the rotation planes normal to it. For example, the rotation planes for the tip fin are normal to the global xy plane.

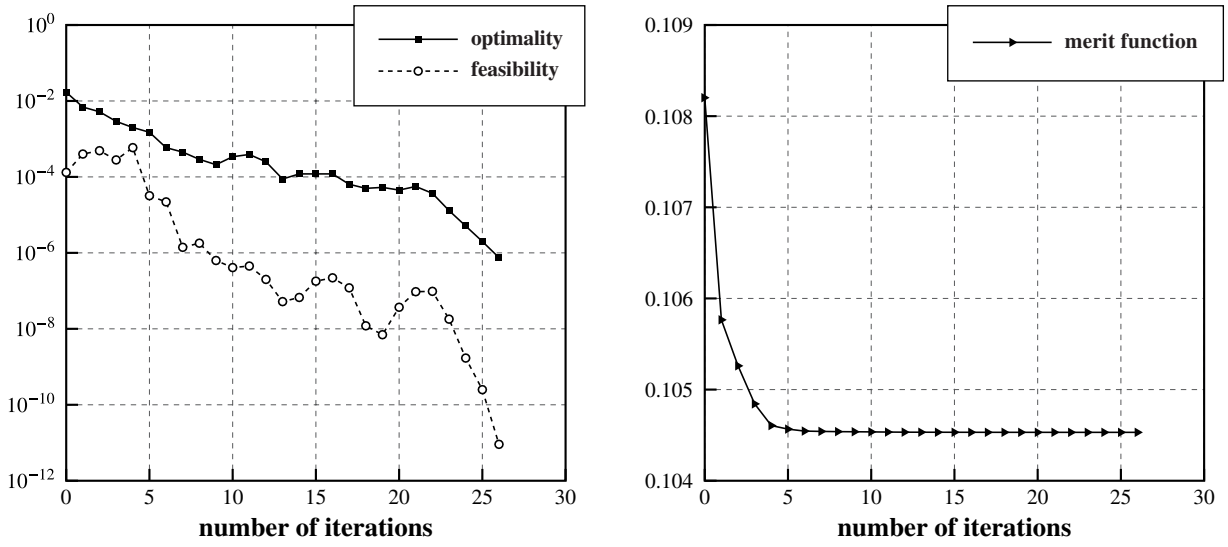

(a) optimality and feasibility

(b) merit function

Fig. 4 Convergence history of the NACA-0012 BW geometry ($C_L = 0.5$, $h/b = 0.20$).

For the corner fillets, the rotation planes are derived from a linear combination of xz and xy planes. The top and bottom wings are each assigned 7 design variables that are evenly distributed on $\eta \in [0, 1]$; similarly, the tip fin is assigned 4 design variables that are evenly distributed on $\eta_V \in [0, 1]$. Each corner fillet has 2 additional design variables that are evenly spaced between its 2 tip design variables. However, in order to prevent wavy surfaces at the corner fillets, here these additional design variables are constrained to linearly interpolate the tip design variables; hence, the optimization problems have effectively 18 design variables each.

All nine optimizations converged to optimality and feasibility tolerances of 10^{-6} and 10^{-7}, respectively, in 28 major SNOPT iterations or less. The convergence history for the case where $C_L = 0.5$ and $h/b = 0.20$ is shown in Fig. 4.

As seen from Fig. 3b, the (inverse) span efficiencies are in good agreement with those estimated by linear theory, i.e. Eq. (3). The discrepancies can be attributed to the definition of h and b in Fig. 3a. If the true bounding boxes of the overall systems are used instead, i.e. when accounting for airfoil thickness, the h/b ratios are in fact slightly larger. Consequently, with the corrected h/b ratios the dashed curve shifts to the right and falls almost exactly on the curve corresponding to Eq. (3).

For the cases where C_L is varied from 0.3 to 0.7 by increments of 0.1 while fixing the h/b ratio at 0.20,

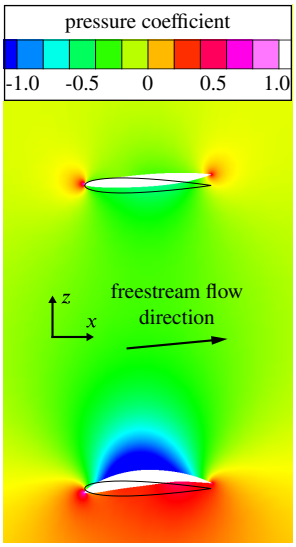

Fig. 5 Plane cut taken at midspan of the $C_L = 0.5^*$ case.

the span efficiencies are $e = 1.54$, 1.51, 1.50, 1.49, and 1.49, respectively. As mentioned in Sec. I, airfoils designed for biplanes should have substantially different camber than those designed for monoplanes [13], thus it should be possible to minimize the influence of C_L on e by enabling sectional shape changes. To get a sense of the performance gain that can be achieved through airfoil tailoring, we repeat the $C_L = 0.5$, $h/b = 0.20$ case but with the addition of sectional shape control on the top and bottom wings. The new case is referred to as $C_L = 0.5^*$. Including twist, the optimization problem has 166 geometric design variables (144 sectional shape design variables). An internal volume inequality constraint with a minimum bound of 99% of the initial internal volume is also enforced. As expected, camber does appear, see Fig. 5, although only on the bottom wing where most of the internal volume is shifted. The top wing twists to face the freestream and its thickness is reduced to the lower bound at the leading edge. The span efficiency of the system is 1.5984, a 6% improvement. Strictly speaking, the comparison is not fair since the leading edge was not constrained, which resulted in a slight increase of h/b. Nevertheless, we consistently observed the same qualitative shape changes as those shown in Fig. 5 when repeating this experiment with varying degrees of freedom.

The sectional force coefficients along the spanwise (vertical) axis of the wings (tip fin) for the cases where C_L is varied and the h/b ratio is fixed at 0.20 are plotted in Fig. 6. Note that the force vectors used to compute these coefficients are not oriented according to the angle of attack, but rather according to the Cartesian axis normal to each surface, i.e. the global z axis for the wings and the global y axis for the tip fin.

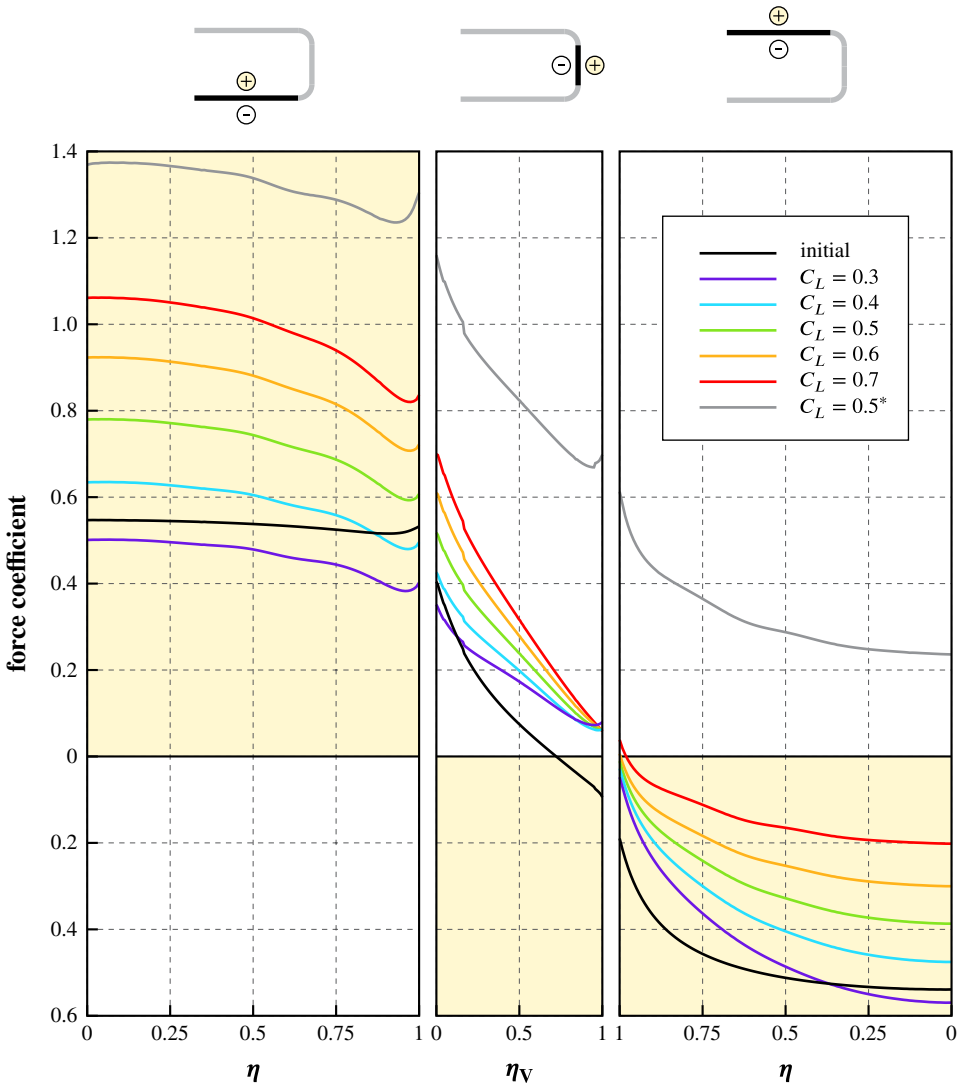

Fig. 6 Optimized force coefficient distributions of the NACA-0012 BW geometry for a range of lift coefficients ($h/b = 0.20$). The $C_L = 0.5^*$ case includes both twist and sectional shape design variables.

Unlike the span efficiencies, the vertical force distributions differ significantly compared to those typically depicted [5, 27]. Here the bottom wing carries significantly more lift than the top wing, although as the lift coefficient decreases the load is progressively shifted to the top wing (relative to a given force distribution). The side-force distribution adapts to this shift while remaining relatively similar in shape, but it never crosses the horizontal axis, even for the $C_L = 0.3$ case where the top and bottom wings carry more or less the same load. Finally, the force distribution of the top wing is more elliptical than that of the bottom wing; in general, it is also smoother.

Also visible in Fig. 6 is the force distribution of the case $C_L = 0.5^*$, which is shifted upward to the point

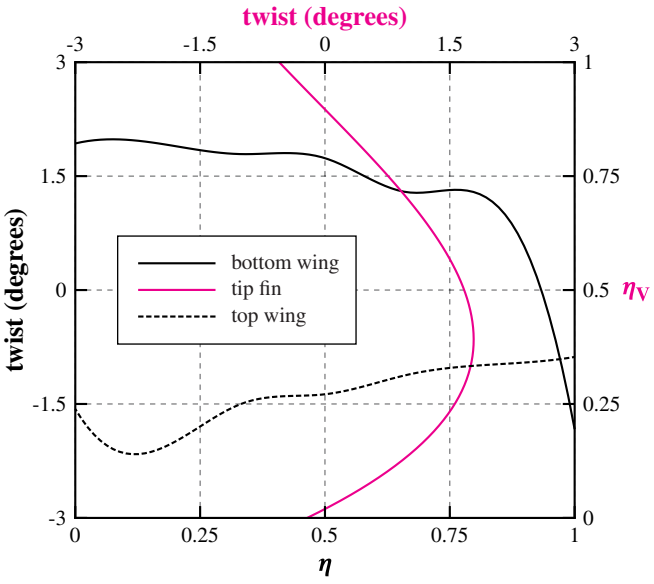

Fig. 7 Optimal twist distribution of the NACA-0012 BW geometry ($C_L = 0.5$, $h/b = 0.20$).

where the top wing carries negative lift throughout its entire span. This result is consistent with lifting-line theory, according to which a vortex loop of constant circulation can be superimposed to a closed system without changing its total lift and drag [2, 28]. This unique property of the BW to redistribute its optimal lift distribution while retaining the expected span efficiency is also apparent from the force distributions of the cases where h/b is varied and C_L is fixed at 0.5. For these cases also, the bottom wing carries significantly more lift, however as the h/b ratio increases the load is again progressively shifted to the top wing; see [26].

It thus appears that, at least from the perspective of linear theory, there are an infinite number of optimally-loaded box wings for a given lift coefficient and h/b ratio. It is, however, unclear whether this holds in the context of nonlinear aerodynamics. As a check for multimodality, we repeated the $C_L = 0.5$, $h/b = 0.20$ case five times, each time with a different starting twist distribution. Specifically, each case was started from a separate set of randomly-generated design variables ranging from $-10°$ to $10°$. All optimizations converged to the same twist distribution shown in Fig. 7 (plus or minus numerical tolerances), implying that the optimal force distribution of the box wing, based on the Euler equations, is unimodal. However, as suggested by the previous cases and in particular the $C_L = 0.5^*$ case, the cost of deviating from this global optimum is small, provided the force distribution is shifted by a constant. This design flexibility gives the BW a substantial advantage over the TW, as discussed in the following studies.

B. Study 1: Twist and Section Design Variables

With confidence in our tools, we now proceed with Study 1 of the transonic BW aircraft configuration. It is the simplest of the five studies, and as such it is intended to serve not only as a baseline but also to answer the questions: when omitting practical constraints, how much is there to gain with the BW relative to the TW? Do compressibility effects overwhelm the potential gain in induced drag?

Only twist and sectional shape design variables are activated, along with the internal volume and lift constraints. Recall from Sec. II B 2 that the BW and reference TW configurations are parameterized with 546 and 214 geometric design variables, respectively. In the following, the definition of the normalized semi-span and vertical coordinates, i.e. η and η_V respectively, is the same as that used for the NACA-0012 BW geometry in Fig. 3a.

The initial flow solution of the BW configuration is smoother overall than that of the TW due to its thinner airfoils, with the exception of a shock wave outboard along the leading edge of the bottom wing, a weak shock wave inboard close to the trailing edge of the bottom wing, and a localized supersonic bubble at the root of the top wing; see Fig. 8. Also shown in Fig. 8 are the wing sections and corresponding pressure coefficient plots of the optimized BW configuration. The shocks have been completely removed as a result of the optimization. The pressure distributions are smoother overall, especially along the leading edge. Along the trailing edge the pressure recovery regions are generally steeper, a typical feature of Euler-based optimizations — with viscous effects the same geometry would likely experience flow separation [29]. The profound impact of the flow field induced by the neighboring wings on their final shape is striking. Similar trends to those observed on the joined wing by Wolkovitch [10] are visible. First, whereas the bottom wing is washed-out (the incidence at Fig. 8d is less than at 8a) the top wing is washed-in (the incidence at Fig. 8l is more than at 8i). Second, the bottom wing incorporates more camber than the top wing.

Comparing the initial (black) and optimized (purple) force distributions in Fig. 9, the optimizer redistributed the load carried by each wing, resulting in a smooth normal force distribution and a final span efficiency of 1.43. According to Eq. (3), the span efficiency of a box wing with an h/b ratio of 0.2 and no dihedral is 1.47. Interestingly, unlike the subsonic NACA-0012 BW optimizations (recall Fig. 6 of Sec. III A), here the optimized force distribution reaches a circulation of zero at about $\eta_V = 0.5$ (as typically depicted [5, 27]). One plausible explanation for this difference is that, despite the transonic speed, here the nonlinear effects

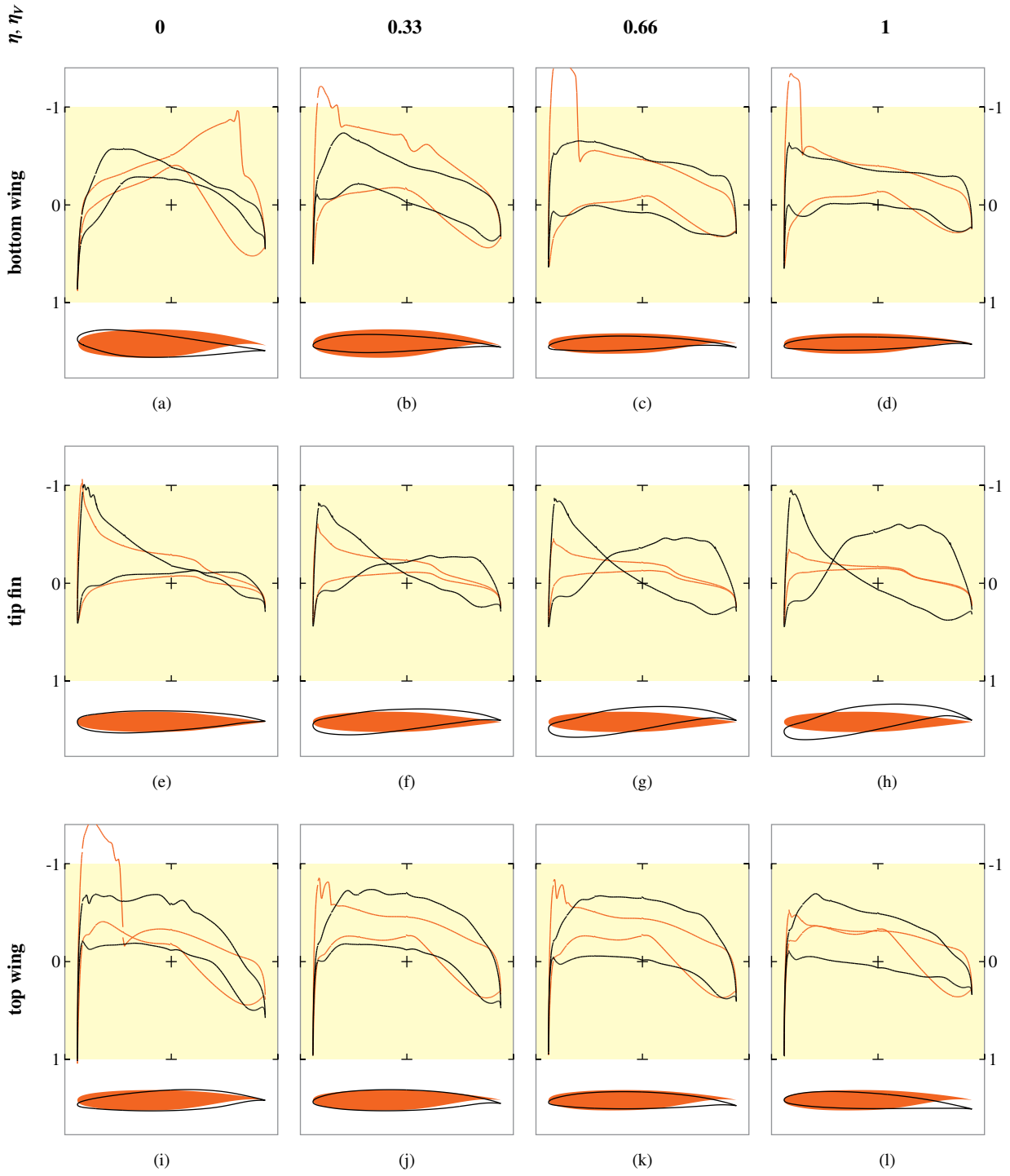

Fig. 8 Pressure coefficient section plots of the BW aircraft configuration; the black lines refer to the optimized sections (Study 1).

are not as severe at the tip since the corner fillets are not only larger (relative to the geometry) but the wing sections there are also considerably thinner (as a result of taper).

A summary of the aerodynamic functionals from the converged optimizations as well as the locations

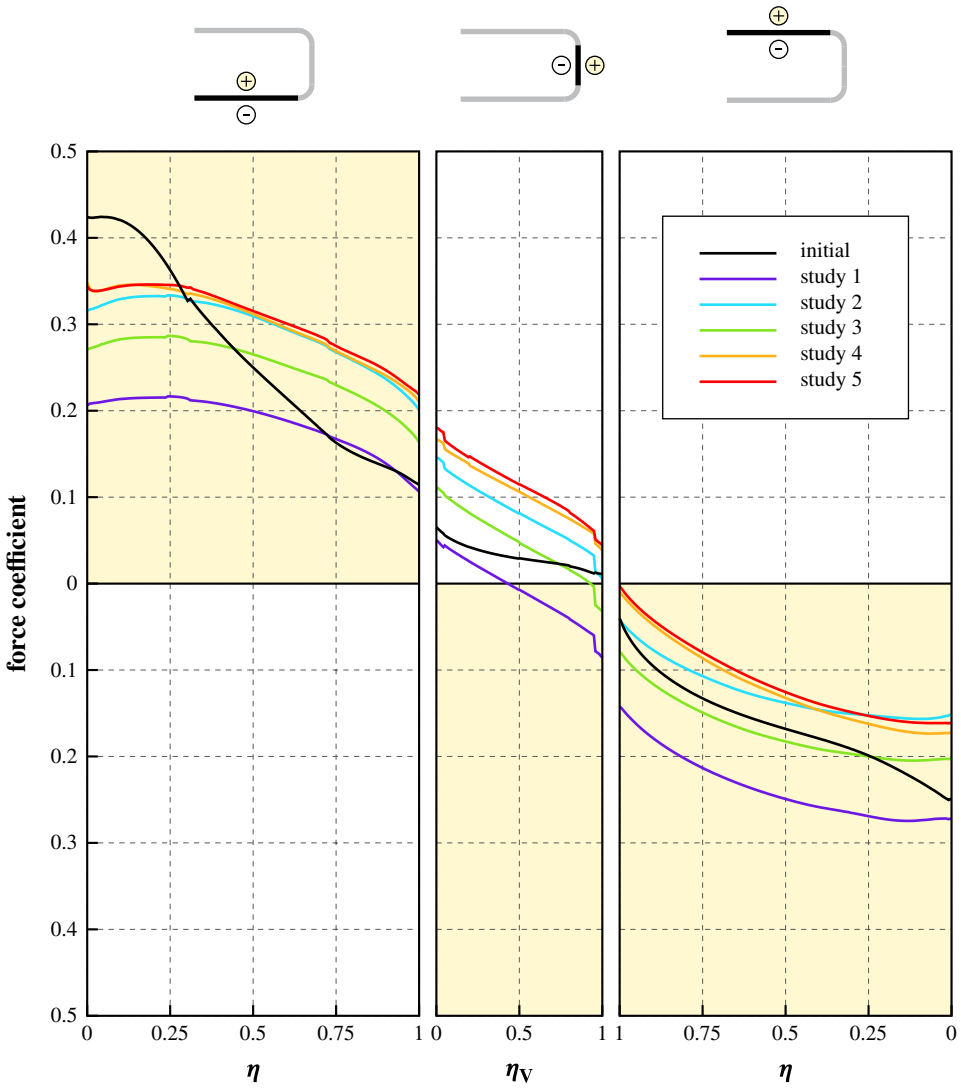

Fig. 9 Optimized force coefficient distributions of the BW aircraft configuration for all five studies.

of the center of gravity and neutral point is given in the first row of Table 3. In this table, the numbers that are highlighted in blue denote quantities that are under direct control by the optimizer — compare with Table 2. The last three columns of the table contain quantities derived from the post-optimization fine-grid flow analyses. Finally, the last column reports the drag reduction of the BW *relative to the similarly optimized reference TW*. In this first study, the span efficiency of the BW is 1.43, and its net drag reduction relative to the TW is 24.8%. Note that, although the center of gravity is well ahead of the neutral point, the final BW configuration is nonetheless unstable since the magnitude of the pitching moment (M_y) is very large.

Table 3 Results of the aerodynamic optimization trade studies

study	$\frac{L}{q_\infty}$ [m^2]	$\frac{D}{q_\infty}$ [m^2]	$\frac{M_y}{q_\infty}$ [m^3]	$\frac{M_x}{q_\infty}$ [m^3]	x_{cg} [m]	$x_{np} - x_{cg}$ [m]	e	$\frac{L}{D}$	ΔD[%]
1	19.6	0.260	−73.6	114.4	10.33	1.85	1.43	78.1	−24.8
2	19.6	0.266	0.0	101.4	10.33	1.57	1.45	79.1	−27.4
3	19.6	0.264	0.0	106.6	11.87	0.18	1.44	78.5	−26.4
4	19.6	0.269	2.4	91.5	10.33	1.47	1.44	78.4	−38.8
5	19.6	0.268	0.0	91.5	10.62	2.08	1.43	78.0	−42.6

[a] The last three columns refer to post-optimization fine-grid flow analyses.

C. Study 2: Trim Constraint

The optimization of Study 1 is now repeated with the addition of a trim constraint. The longitudinal location of the center of gravity is still fixed at 10.33 m; see Table 1 and Fig. 2.

Based on the discussion of Sec. III A, it should be possible for the optimizer to trim the BW configuration by simply adjusting the magnitude of the constant circulation loop to add an arbitrary moment to the design without an induced drag penalty. This is precisely what can be observed from Fig. 9: the shape of the Study 2 curve is essentially the same as the Study 1 curve, but since the center of gravity is closer to the front wing the optimizer shifted the Study 1 curve upward by a constant to trim the aircraft. The TW configuration, on the other hand, is forced to carry negative lift on its horizontal tail as the optimizer reaches the geometric bounds on the main wing [15]. As a result, the TW incurs a higher penalty for the trim constraint than the BW. Relative to Study 1, the TW is about 3% less efficient, whereas the BW is about 1% more efficient (when analyzed on the fine grid). Hence, in the current study the efficiency gain of the BW over the TW is roughly 27.4% (see Table 3).

In this study, as well as in the other remaining studies, the wing sections of the optimized BW configuration are very similar to those already shown in Fig. 8.

D. Study 3: Center of Gravity Design Variable and Static Margin Constraint

The BW configuration that resulted from Study 2 is longitudinally stable even though no static margin constraint was imposed. To investigate whether drag reductions can be achieved by relocating the center of

gravity, the optimization of Study 2 is now repeated with the addition of x_{cg} as a design variable. A static margin of $0.05c$ (0.18 m) is enforced to ensure that the design remains stable. For the TW the lower bound on the static margin is also $0.05c$ (0.29 m), but x_{cg} is limited to an upper bound of 33% of the mean aerodynamic chord. There is no such bound on x_{cg} for the BW.

As the simulation progressed, the optimizer moved the center of gravity aft by 1.54 m, which allowed it to shift the force distribution of Study 2 back toward the force distribution of Study 1. However in the process it quickly reached the bound on the static margin, which remained active until the end of the optimization. As seen from Fig. 9, approximately 60% of the total lift produced by the final configuration is carried by the bottom wing, which is consistent with the findings of Rizzo and Frediani [30]. However, once analyzed with the fine grid the final configuration is no longer superior than the optimized configuration of Study 2. Hence, at least from the perspective of inviscid drag, it appears that the stability of the BW can be ensured at no performance cost by simply positioning the center of gravity toward the front wing.

In the case of the TW optimization, the optimizer also quickly reached the upper bound of x_{cg}, which gave it enough freedom to even surpass the minimum stability requirement while also loading the horizontal tail with positive lift. For this reason the drag reduction of the BW relative to the TW is slightly smaller than in Study 2.

E. Study 4: Bending Moment Constraint

We now investigate the trade-off between drag and the optimal force distribution when the latter is constrained to generate a center-plane bending moment that is less than or equal to 80% of the center-plane bending moment generated by a force distribution optimized for minimum drag but without a bending moment constraint. Here the reference force distributions of the BW and TW configurations are those resulting from Study 1.

As explained in Sec. II B 3, the intent of this study is to retrieve a force distribution that is closer to an aerostructural optimum without explicitly modeling structures. It is important to realize that the bending moment constraint only acts as a surrogate; in particular, wing deflection is not captured.

As expected from the TW, the lift distribution resulting from this study is triangular and thus far from the ideal elliptical distribution [21]. In the case of the BW, the shape of the force distribution is almost unchanged

relative to Study 1; relative to Study 2, the biggest discrepancy is on the top wing where the force distributions cross each other, i.e. the force distribution there is slightly shifted inboard. The final span efficiency and lift-to-drag ratio are, however, virtually unchanged from the previous studies. Hence, a substantial performance gain is achieved by the BW over the reference TW; compared with Study 1, the performance gain resulting from the bending moment constraint alone is 14.0% (see Table 3). We reiterate that it is unclear whether the bending moment constraint constitutes a realistic or even a valid assumption when applied to the BW configuration.

F. Study 5: Planform Design Variables

The final study is cumulative in that it includes all the design variables and all the constraints considered so far. Given that the initial planform of the BW has not been sized with high-fidelity tools, we activate the leading edge sweep of both the top and bottom wings as design variables. The sweep of both wings can change by plus or minus 5°. Other planform parameters such as taper and dihedral remain fixed.

Once again the optimizer successfully satisfied all constraints without penalizing the performance of the final BW. By the end of the optimization the top wing is swept forward by less than 1° and the bottom wing is swept backward by the maximum amount of 5°, corresponding to an x-directional translation of roughly $0.58c$. The initial and final BW configurations are pictured in Fig. 10 where the signature of the trailing vortices is illustrated in each case by the vertical component of momentum. The induced velocities are considerably smaller for the final BW configuration, an indicator that the force distribution has reached an optimum. As seen from Fig. 9, the force distribution is indeed similar in shape to those of all four previous studies, and is almost exactly identical in shape and magnitude to Study 4. The driving design parameter in this study is thus the bending moment constraint. Compared with Study 3, the center of gravity also moved back but not as much, remaining well ahead of the neutral point leading to a very stable configuration. In the case of the reference TW, the optimizer could also satisfy all constraints but at the expense of producing 42.6% more drag than the BW.

IV. Conclusions and Future Work

This work studied the aerodynamic trade-offs of a transonic box-wing regional jet configuration using high-fidelity computational fluid dynamics and optimization.

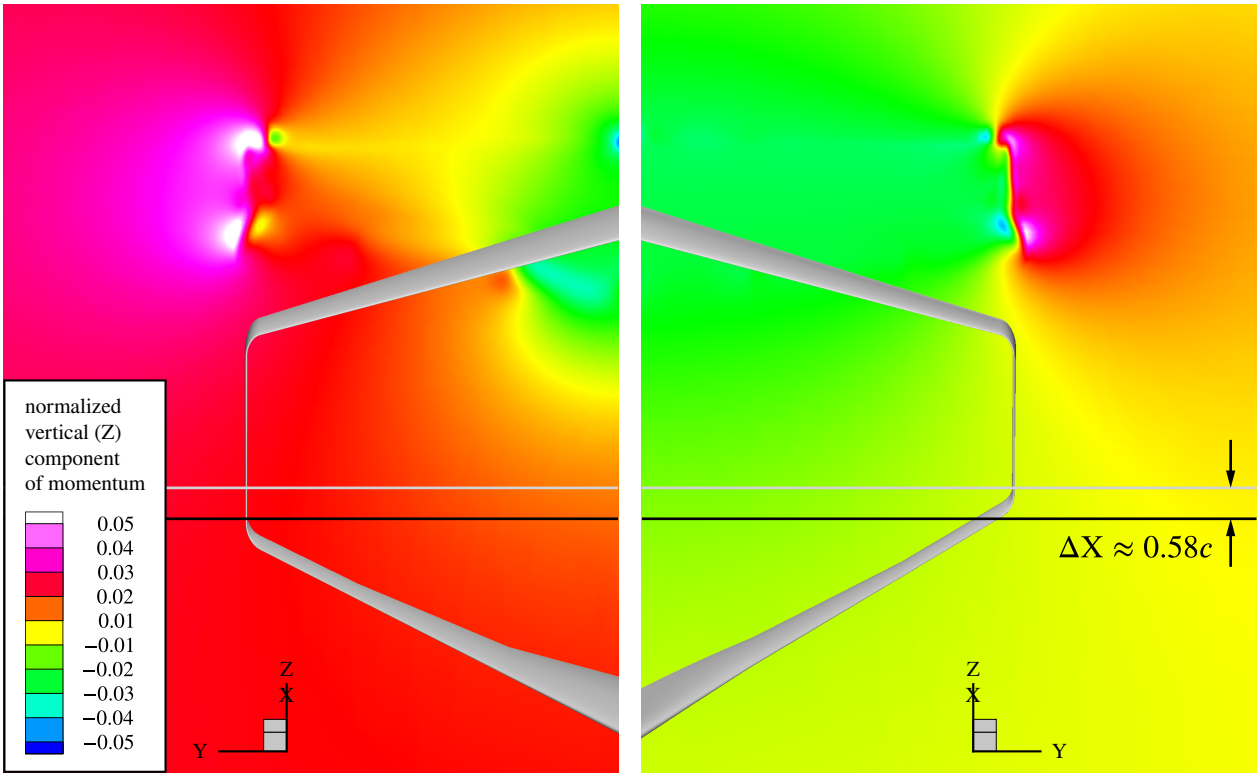

(a) initial

(b) optimized

Fig. 10 Plane cuts of the vertical component of momentum taken at 1 root-chord length downstream of the initial and optimized BW aircraft configurations (Study 5).

The influence of nonlinear physics on the aerodynamics of the box wing was first investigated by optimizing a simple NACA-0012 box-wing geometry at subsonic speed under a range of lift coefficients and height-to-span ratios. While the resulting span efficiencies are in excellent agreement with those estimated by linear theory, the optimal force distributions do not correspond to those typically depicted [5, 27]. In particular, the circulation of an optimally-loaded box wing does not necessarily reach zero at midheight of the vertical tip fins. Rather, the optimal force distribution is unique to each combination of lift coefficient and height-to-span ratio. That being said, as remarked in Kroo [2], it is possible to shift the optimal force distribution of the box wing by a constant circulation loop with minimal impact on drag. This feature is central to the transonic trade studies that follow.

Five transonic studies were conducted, where each study was subject to a different combination of twist, section, sweep, and balance design variables, as well as volume, lift, trim, bending moment, and stability constraints. Equivalent studies were conducted on a reference tube-and-wing configuration. On the basis of

inviscid pressure drag, the box wing considered here is up to 42.6% more efficient than the tube-and-wing. Roughly 2.6% and 14.0% of this gain results from the imposition of a trim and bending moment constraints, respectively. In each case the efficiency gain is attributable to the unique capability of the box wing to shift its optimal lift distribution in order to meet the specified constraints but without degrading its efficiency. The box wing also appears to be remarkably stable relative to the tube-and-wing, which is desirable for safety reasons.

We stress that the drag reductions reported here are based on inviscid simulations, and that the implications of the bending moment constraint as a surrogate for a structural model are unknown in the context of a box-wing configuration. Further, many other important issues remain to be studied. For example, even though the box wing studied here has the same span and wetted area as the reference tube-and-wing configuration, its viscous drag is expected to be larger due to its shorter chords (unless laminar flow technology is assumed, in which case the box wing could be favored). Finally, and more importantly, if the box wing is to ever become the future of commercial transport, its wing structure must be at least as light as that of a tube-and-wing while being stiff enough to address the many concerns over its undesirable aeroelastic characteristics such as early flutter onset.

Acknowledgments

The authors are thankful for the financial support provided by the Ontario Graduate Scholarship in conjunction with the University of Toronto. Computations were performed on the General Purpose Cluster supercomputer at the SciNet High Performance Computing Consortium.

References

[1] Prandtl, L., "Induced Drag of Multiplanes," Tech. Rep. TN-182, NACA, 1924.

[2] Kroo, I., "Drag Due to Lift: Concepts for Prediction and Reduction," *Annual Review of Fluid Mechanics*, Vol. 33, 2001, pp. 587–617,
doi:10.1146/annurev.fluid.33.1.587.

[3] Lee, D. S., Pitari, G., Grewe, V., Gierens, K., Penner, J. E., Petzold, A., Prather, M. J., Schumann, U., Bais, A., Berntsen, T., Iachetti, D., Lim, L. L., and Sausen, R., "Transport impacts on atmosphere and climate: Aviation," *Atmospheric Environment*, Vol. 44, No. 37, 2010, pp. 4678–4734,
doi:10.1016/j.atmosenv.2009.06.005.

[4] Miranda, L. R., "Boxplane Configuration – Conceptual Analysis and Initial Experimental Verification," Tech. Rep. LR-25180, Lockheed-California Company, 1972.

[5] Lange, R. H., Cahill, J. F., Bradley, E. S., Eudaily, R. R., Jenness, C. M., and MacWilkinson, D. G., "Feasibility study of the transonic biplane concept for transport aircraft application," Tech. Rep. NASA-CR-132462, Lockheed-Georgia Company, 1974.

[6] Frediani, A., "The Prandtl wing," in Torenbeek, E. and Deconinck, H., eds., "Innovative configurations and advanced concepts for future civil transport aircraft," von Karman Institute, VKI Lecture Series, 2005.

[7] Frediani, A. and Cipolla, V., "The PrandtlPlane Configuration: Overview on Possible Applications to Civil Aviation," in Buttazzo, G. and Frediani, A., eds., "Variational Analysis and Aerospace Engineering: Mathematical Challenges for Aerospace Design," Springer US, Vol. 66 of *Springer Optimization and Its Applications*, pp. 179–210, 2012,
doi:10.1007/978-1-4614-2435-2_8.

[8] Divoux, N. and Frediani, A., "The Lifting System of a PrandtlPlane, Part 2: Preliminary Study on Flutter Characteristics," in Buttazzo, G. and Frediani, A., eds., "Variational Analysis and Aerospace Engineering: Mathematical Challenges for Aerospace Design," Springer US, Vol. 66 of *Springer Optimization and Its Applications*, pp. 235–267, 2012,
doi:10.1007/978-1-4614-2435-2_10.

[9] Dal Canto, D., Frediani, A., Ghiringhelli, G. L., and Terraneo, M., "The Lifting System of a PrandtlPlane, Part 1: Design and Analysis of a Light Alloy Structural Solution," in Buttazzo, G. and Frediani, A., eds., "Variational Analysis and Aerospace Engineering: Mathematical Challenges for Aerospace Design," Springer US, Vol. 66 of *Springer Optimization and Its Applications*, pp. 211–234, 2012,
doi:10.1007/978-1-4614-2435-2_9.

[10] Wolkovitch, J., "The joined wing: An overview," *Journal of Aircraft*, Vol. 23, No. 3, 1986, pp. 161–178,

doi:10.2514/3.45285.

[11] Frediani, A., Quattrone, F., and Contini, F., "The Lifting System of a PrandtlPlane, Part 3: Structures Made in Composites," in Buttazzo, G. and Frediani, A., eds., "Variational Analysis and Aerospace Engineering: Mathematical Challenges for Aerospace Design," Springer US, Vol. 66 of *Springer Optimization and Its Applications*, pp. 269–288, 2012,
doi:10.1007/978-1-4614-2435-2_11.

[12] Demasi, L., Cavallaro, R., and Razón, A. M., "Postcritical Analysis of PrandtlPlane Joined-Wing Configurations," *AIAA Journal*, Vol. 51, No. 1, 2013, pp. 161–177,
doi:10.2514/1.J051700.

[13] Addoms, R. B. and Spaid, F. W., "Aerodynamic Design of High-Performance Biplane Wings," *Journal of Aircraft*, Vol. 12, No. 8, 1975, pp. 629–630,
doi:10.2514/3.59846.

[14] Munk, M. M., "The Minimum Induced Drag of Aerofoils," Tech. Rep. TR-121, NACA, 1923.

[15] Gagnon, H. and Zingg, D. W., "High-Fidelity Aerodynamic Shape Optimization of Unconventional Aircraft Through Axial Deformation," in "52nd Aerospace Sciences Meeting," National Harbor, Maryland, AIAA Paper 2014-0908, 2014,
doi:10.2514/6.2014-0908.

[16] Raymer, D. P., *Aircraft Design: A Conceptual Approach*, AIAA Education Series, AIAA, Reston, 5th ed., 2012.

[17] Gagnon, H. and Zingg, D. W., "Geometry Generation of Complex Unconventional Aircraft with Application to High-Fidelity Aerodynamic Shape Optimization," in "21st AIAA Computational Fluid Dynamics Conference," San Diego, California, AIAA Paper 2013-2850, 2013,
doi:10.2514/6.2013-2850.

[18] Whitcomb, R. T., "Review of NASA supercritical airfoils," in "9th Congress of the International Council of the Aeronautical Sciences," Haifa, Isreal, 1974.

[19] Mader, C. A. and Martins, J. R. R. A., "Stability-Constrained Aerodynamic Shape Optimization of Flying Wings," *Journal of Aircraft*, Vol. 50, No. 5, 2013, p. 5,
doi:10.2514/1.C031956.

[20] Zhang, Z. J., Khosravi, S., and Zingg, D. W., "High-Fidelity Aerostructural Optimization with Integrated Geometry Parameterization and Mesh Movement," in "56th AIAA/ASCE/AHS/ASC Structures, Structural Dynamics, and Materials Conference," Kissimmee, Florida, AIAA Paper 2015-1132, 2015,
doi:10.2514/6.2015-1132.

[21] Jones, R. T., "The Spanwise Distribution of Lift for Minimum Induced Drag of Wings Having a Given Lift and a

Given Bending Moment," Tech. Rep. TN-2249, NACA, 1950.

[22] Hicken, J. E. and Zingg, D. W., "Aerodynamic Optimization Algorithm with Integrated Geometry Parameterization and Mesh Movement," *AIAA Journal*, Vol. 48, No. 2, 2010, pp. 400–413, doi:10.2514/1.44033.

[23] Gagnon, H. and Zingg, D. W., "Two-Level Free-Form and Axial Deformation for Exploratory Aerodynamic Shape Optimization," *AIAA Journal*, Vol. 53, No. 7, 2015, pp. 2015–2026, doi:10.2514/1.J053575.

[24] Hicken, J. E. and Zingg, D. W., "Parallel Newton-Krylov Solver for the Euler Equations Discretized Using Simultaneous-Approximation Terms," *AIAA Journal*, Vol. 46, No. 11, 2008, pp. 2273–2786, doi:10.2514/1.34810.

[25] Gill, P. E., Murray, W., and Saunders, M. A., "SNOPT: An SQP Algorithm for Large-Scale Constrained Optimization," *SIAM Review*, Vol. 47, No. 1, 2005, pp. 99–131, doi:10.1137/S0036144504446096.

[26] Lee, C., Koo, D., Telidetzki, K., Buckley, H., Gagnon, H., and Zingg, D. W., "Aerodynamic Shape Optimization of Benchmark Problems Using Jetstream," in "53rd AIAA Aerospace Sciences Meeting," Kissimmee, Florida, AIAA Paper 2015-0262, 2015, doi:10.2514/6.2015-0262.

[27] Frediani, A. and Montanari, G., "Best wing system: an exact solution of the Prandtl's problem," in Buttazzo, G. and Frediani, A., eds., "Variational Analysis and Aerospace Engineering," Springer New York, Vol. 33 of *Springer Optimization and Its Applications*, pp. 183–211, 2009, doi:10.1007/978-0-387-95857-6_11.

[28] Demasi, L., Dipace, A., Monegato, G., and Cavallaro, R., "Invariant Formulation for the Minimum Induced Drag Conditions of Nonplanar Wing Systems," *AIAA Journal*, Vol. 52, No. 10, 2014, pp. 2223–2240, doi:10.2514/1.J052837.

[29] Osusky, L., Buckley, H., Reist, T., and Zingg, D. W., "Drag Minimization Based on the Navier-Stokes Equations Using a Newton-Krylov Approach," *AIAA Journal*, Vol. 53, No. 6, 2015, pp. 1555–1577, doi:10.2514/1.J053457.

[30] Rizzo, E. and Frediani, A., "Application of Optimisation Algorithms to Aircraft Aerodynamics," in Buttazzo, G. and Frediani, A., eds., "Variational Analysis and Aerospace Engineering," Springer New York, Vol. 33 of *Springer Optimization and Its Applications*, pp. 419–446, 2009, doi:10.1007/978-0-387-95857-6_23.